Received: 28 June 2024 | Revised: 31 July 2024 | Accepted: 7 August 2024

DOI: 10.1002/rcm.9895

RESEARCH ARTICLE

Rapid Communications in Mass Spectrometry WILEY

Investigation of the laser fluence and wavelength dependence in surface-assisted laser desorption/ionization mass spectrometry using gold nanoparticles

Wendy H. Müller[1,2] | Alexander Potthoff[1] | Klaus Dreisewerd[1] | Jens Soltwisch[1]

[1]Institute of Hygiene, University of Münster, Münster, Germany

[2]Mass Spectrometry Laboratory, MolSys Research Unit, Department of Chemistry, University of Liège, Liège, Belgium

Correspondence
Wendy H. Müller, Mass Spectrometry Laboratory, MolSys Research Unit, Department of Chemistry, University of Liège, Allée du Six Août,11 - Quartier Agora, 4000 Liège, Belgium.
Email: wmuller@uliege.be

Jens Soltwisch, Institute of Hygiene, University of Münster, Robert-Koch-Str. 41, 48149 Münster, Germany.
Email: jens.soltwisch@ukmuenster.de

Funding information
Alexander von Humboldt Foundation

Rationale: Surface-assisted laser desorption/ionization (SALDI) mass spectrometry (MS) builds on the use of nanostructured surfaces (e.g., coatings of colloidal nanoparticles) to promote analyte desorption and ionization. The SALDI process is believed to occur mainly through thermal processes, resulting from heating of the nanosubstrate upon absorption of the photon energy, and by assisting ionization steps. Mostly due to the accessibility of the respective hardware, the majority of SALDI-MS studies use standard laser wavelengths for MALDI (i.e., 337 or 355 nm), even though peak absorption of the SALDI nanosubstrate might completely differ from these values.

Methods: Here, we investigated the wavelength dependence in SALDI-MS to determine if wavelength adjustment would be beneficial, and to provide new experimental data for a better understanding of the SALDI mechanism. To this end, gold nanoparticles (AuNPs) sprayed onto microscope glass slides were employed as SALDI nanosubstrates and L-arginine as a model analyte. In addition, we used 2,5-dihydroxyacetophenone (2,5-DHAP) for classical MALDI-MS using the same experimental setup. Arginine ion signals were recorded as a function of laser wavelength and laser fluence. Mass spectra were acquired in the wavelength range between 310 and 630 nm, including the absorption maximum of the sprayed AuNPs around 550 nm and that of 2,5-DHAP around 380 nm.

Results: Laser fluence thresholds for the generation of arginine ions were found to be dependent on the laser wavelength and to inversely correlate with the absorbance profiles of the deposited AuNPs and 2,5-DHAP, respectively. Very differently to MALDI, in SALDI ionization efficiency was found to strictly linearly decrease with increasing laser wavelength.

Conclusions: Our results, therefore, corroborate the general assumption that material ejection in SALDI-MS is mainly driven by thermal processes in the low laser fluence range and add new evidence that the ionization process is directly influenced by photon energy when AuNPs are employed as nanosubstrates.

1 | INTRODUCTION

Matrix-assisted laser desorption/ionization mass spectrometry (MALDI-MS), developed in the late 1980s,[1] has rapidly become popular due to its low detection limits, its robustness, its high-throughput capacity, and its ability to analyze a broad range of compounds classes,[2] in "soft" conditions (enabling to minimize fragmentation of large labile biomolecules, compared to harder ionization techniques like electron ionization). The main difference between MALDI and previous laser ionization techniques is the introduction of a "matrix",[3] which is typically a low-molecular-weight organic compound, able to co-crystallize with the molecules present in the sample and, bearing a suitable chromophore, effectively absorbing the laser light (in UV-MALDI). The main roles of the MALDI matrix consist in preventing aggregation by isolating the analytes from each other, protecting the analytes from direct laser irradiation (limiting their fragmentation), assisting the desorption through the absorption of the laser energy and its transfer to the analytes, and promoting efficient ionization of the analytes (usually by [de] protonation).[4] Along with the development of the MALDI-MS technique, a multitude of organic matrices have been proposed, each with its own (dis)advantages.[2,5]

An alternative technique to classical MALDI is surface-assisted laser desorption/ionization (SALDI) MS.[6–10] This technique relies on the use of a nanostructured surface, with which the analytes are directly in contact. Examples of SALDI nanosubstrates comprise coatings of colloidal nanoparticles, nanostructured solid supports, or sputtered metal nanoclusters.[8] Like the matrix in MALDI-MS, the nanosubstrates play a key role in the convoluted SALDI desorption/ionization processes. In SALDI-MS, in particular, the rapid rise in the nanosubstrate surface temperature upon absorption of the laser photons is believed to play a decisive role in the desorption mechanism.[8,11] Hence, the nanosubstrate characteristics (e.g., bulk composition, surface chemistry, and morphology[12]) critically affect the SALDI-MS performance. However, the understanding of the fundamental mechanisms underlying the ionization and analyte transfer into the gas phase in both LDI-derived MS techniques (i.e., MALDI and SALDI) is still a significant challenge. Nevertheless, several fundamental studies focused on the desorption/ionization processes, in MALDI-MS[4,13–18] and SALDI-MS.[8,19–21] In the past, attempts have been made in MALDI-MS to rationalize the impact of important parameters related to the instrumentation, and in particular, to the laser irradiation, such as the laser wavelength, fluence, pulse duration, and beam profile.[4,22–28] For example, numerous studies have demonstrated that optimal analytical results are obtained if the irradiation laser wavelength matches the absorption band of the MALDI matrix in the solid state.[3,4,22–24,29] On the contrary, MALDI-MS performance usually drops when the matrix only exhibits low optical absorption at the excitation wavelength.[24] However, standard MALDI-MS instrumentation usually employs one of two common ns-pulsed lasers with fixed emission wavelengths, i.e., 337 nm (N_2 laser) and 355 nm (frequency-tripled Nd:YAG laser). As a third alternative, frequency-tripled Nd:YLF lasers (349 nm) are also used. As a consequence, many compounds with potentially beneficial matrix properties cannot be used to their full potential because of insufficient optical absorptivity at the excitation laser wavelength.[24] While the interaction between the laser wavelength and the absorption profile of the matrix has been widely studied and proved to be a crucial factor in MALDI-MS,[22–24,29] very few, if any, fundamental studies have been carried out in SALDI-MS, especially to examine the influence of the laser wavelength on the SALDI performance. Currently, the vast majority of SALDI-MS studies use the standard 337, 349, or 355 nm wavelengths, even though the peak absorption of the SALDI nanosubstrate might differ from these values.

In this study, we employed a wavelength-tunable optical parametric oscillator (OPO) laser system coupled to an orthogonal extracting time-of-flight (QTOF) mass spectrometer to investigate the laser intensity and wavelength dependence on the SALDI process for the analysis of the amino acid L-arginine between 310 and 630 nm. We compared colloidal gold nanoparticles (AuNPs) prepared as nanosubstrates on a glass surface in SALDI-MS to 2,5-dihydroxyacetophenone (2,5-DHAP) used as a matrix in MALDI-MS. Our study aimed at determining if wavelength adjustment would be beneficial for SALDI-MS studies, and at providing new experimental data that offer new insights into the SALDI fundamental mechanisms.

2 | EXPERIMENTAL SECTION

2.1 | Chemicals and materials

Ultrapure water was purchased from Carl Roth GmbH (*Karlsruhe, Germany*). Colloidal spherical citrate-coated 30 nm gold nanoparticles (AuNPs) dispersed in water were purchased from NanoQoloids (*Ghislenghien, Belgium*) at a concentration of $2.5x10^{11}$ NPs/mL. Unless otherwise stated, all other chemicals were purchased from Sigma-Aldrich (*Steinheim, Germany*).

2.2 | Sample preparation

The uniform spray deposition of the AuNPs and L-Arginine (BioUltra, ≥ 99.5%) on Superfrost™ glass slides (*Epredia, Braunschweig, Germany*) was performed using an ultrasonic spray coater (*SimCoat, Sono-Tek, Milton, NY*) equipped with an AccuMist nozzle. The AuNPs were centrifuged and resuspended in a mixture of acetonitrile (ACN):H_2O (vol/vol 1:1) at a concentration of 5.00×10^{11} NPs/mL. First, approximately 320 µl of the AuNPs suspension were sprayed on a total surface of 30 × 30 mm (with aline spacing of 1.8 mm) at a flow rate of 50 µl/min and using 50% of the total ultrasonic power, an ultrasonic frequency of 48 kHz, and a N_2 back pressure of approximately 1 bar. In total, 10 layers of AuNPs without drying phases were sprayed on the glass slide. The duration of the AuNPs spraying was approximately 6 minutes. Subsequently, approximately

320 µl of a 1mM L-arginine ACN:H_2O (vol/vol 1:1) solution were sprayed over the produced AuNPs coating using the same settings, with the exception of a value of 55% for the ultrasonic power. A few modifications have been made to prepare the samples for MALDI-MS experiments. L-Arginine was first sprayed on the glass slide using the previously described settings, then approximately 320 µl of a 8 mg/ml ACN:H_2O (vol/vol 1:1) solution of 2,5-dihydroxyacetophenone (2,5-DHAP) (for synthesis) was sprayed over the L-arginine coating using the same settings.

2.3 | UV–visible spectroscopy

UV–visible spectra of the gold nanoparticles in suspension were acquired using a single monochromator UV-2600i spectrophotometer (*Shimadzu*, *Duisburg*, *Germany*). UV–Visible spectra of the AuNPs coating on the glass slide were measured in diffusive reflection mode using an integrating sphere (*ISR-2600Plus*, *Shimadzu*). 2,5-DHAP solution absorption spectra were recorded using a dual-beam spectrophotometer (*UV-2102PC*, *Shimadzu*, *Duisburg*, *Germany*). Solid phase absorption spectra of the matrix were measured in diffusive reflection mode using an integrating sphere (*ISR-260*, *Shimadzu*). In total, 50 mg of matrix powder was mixed with 500 mg of $BaSO_4$, finely ground in a ball mill (*Perkin-Elmer*, *Waltham*, *MA*), and pressed into a pellet. A neat $BaSO_4$ pellet served as the reference.

2.4 | Scanning electron microscopy

Samples were mounted on a standard aluminum SEM-stub by carbon adhesive. After coating with 1.5 nm Pt/C under 45°, followed by rotary shadowing with 2 nm PT/C (Leica ACE 900) images were taken by a field emission SEM (*Hitachi S4700*) equipped with a digital scanning acquisition system (DISS5 point electronic).

2.5 | Mass spectrometry instrumentation and laser systems

Mass spectrometry experiments were carried out on a hybrid, orthogonal-extracting time-of-flight mass spectrometer (MALDI Synapt G2-S HDMS, *Waters/Micromass*, *Manchester*, *UK*), equipped with a modified ion source.[30] A wavelength-tunable optical parametric oscillator (OPO) laser system (*versaScan/170/MB-ULD*, *GWU-Lasertechnik*, *Erftstadt*, *Germany*, pulse duration: 6–7 ns, f_{rep}: 10 Hz) served as the laser irradiation source. The OPO is equipped with a second harmonic generator (SHG), and is pumped by the frequency-tripled beam ($\lambda = 355$ nm) of a Q-switched Nd:YAG laser (*Surelite II-10*, *Continuum/Quantronix*, *Planegg*, *Germany*). The OPO output beam was coupled to the ion source via fiber optics (UV200/220P/NS, *Ceram Optec*, *Bonn*, *Germany*, core/clad diameter: 200/220 µm), producing a flat-top beam intensity profile similar to a setup previously used by Soltwisch et al.[22] The end surface of the fiber was imaged onto the sample surface 1:1 using telescope optics. The wavelength of the OPO laser beam was controlled through ScanMaster software (*GWU-Lasertechnik*, *Erftstadt*, *Germany*). Other parameters (e.g., laser intensity, buffer gas pressure) were controlled using LabVIEW-based software (*National Instruments*, *Austin*, *TX*), as described in detail in Potthoff et al.[30] The LabVIEW-based software also allowed to monitor the laser pulse energies online during the experiments using a beam splitter and a calibrated pyroelectric detector (*model 420*, *Eltec/Silverlight*, *Winterthur*, *Switzerland*, amended with custom-made amplifying circuits). The readouts were registered and recorded with a digital oscilloscope (*PicoScope 2204A*, *Pico Technology*, *St Neots*, *UK*).

2.6 | Laser energy calibration and laser fluence determination

After each change of the OPO output wavelength, calibration of the laser energy was necessary. To this end, the voltage recorded by the digital oscilloscope through the pyroelectric detector was calibrated against the pulse energy, averaged over 10 seconds, recorded by a commercial energy meter (*STARLITE METER*, *OPHIR Photonics*, *Jerusalem*, *Israel*), placed behind the exit of the fiber. Then, laser fluences were calculated by dividing the laser pulse energies delivered to the sample by the laser spot size. Laser spot size measurements were obtained from ablation marks of the black ink of a permanent marker (*Corporate Express*) covering the label area of a Superfrost™ glass slide. The length of the major and minor axes of the ellipses constituting the ablation marks was measured using an Olympus SLIDEVIEW VS200 slide scanner (*Hamburg*, *Germany*).

2.7 | Mass spectra acquisition

Mass spectra were acquired in the positive ionization mode. At a defined laser wavelength, protonated arginine ion signals ($[M + H]^+$, *m/z* 175.1) were recorded as a function of the laser fluence (between 20 and 90% of the maximum available laser intensity). Measurements were conducted at different laser wavelengths, namely 310, 337, 380, 430, 480, 529, 580, and 630 nm. All measurements were recorded via an automated measurement sequence using a setup that combines hardware components with LabVIEW-based software (*National Instruments*, *Austin*, *TX*) for controlling the relevant input parameters. The detailed LabVIEW-based data acquisition strategy is described in Potthoff et al.[30] The datasets were recorded using the standard imaging workflow of the HD imaging and Mass Lynx software (*Waters*). During the data acquisition, the sample plate was moved continuously such that fresh sample areas were scanned for each irradiated pixel. Ion images were recorded at 300×300 µm^2 pixel size in a mass range from *m/z* 50 to 600. During the measurement sequence, the ablation laser intensity was changed using a motor-driven circular neutral density gradient filter (*OptoSigma*, *Santa Ana*, *CA*, *USA*). Buffer gas (N_2) pressure was set to

2 mbar for all measurements. Ten pixels were acquired per laser intensity, and the measurement sequence for one defined wavelength was repeated three times. The MS data were converted to mzML format using ProteoWizard software,[31] and subsequently to imzML format[32] using the imzML converter developed by Race et al.[33] Finally, detector readouts and experimental settings were postprocessed and combined with the MS data, using an in-house Python script and the pyimzML package.[34]

2.8 | Safety Hazard note

The employed lasers are of laser safety class 4. Safety precautions have to be taken upon working with free beams of these lasers (e.g., by wearing protective goggles).

3 | RESULTS AND DISCUSSION

3.1 | Absorption profiles in the liquid and solid states

Absorption profiles of the 2,5-DHAP matrix (in the liquid and solid states), and of the AuNPs (in suspension and when sprayed on a microscope glass slide) are shown in Figures 1 and 2, respectively. As already demonstrated in previous studies, the absorption profile of the matrix is broadened, and a redshift of the peak absorption is observed in the solid state compared to the liquid phase (Figure 1), because of modified intermolecular forces.[23,24,29] The spectrophotometric measurements place the peak absorption of 2,5-DHAP in the solid state at 380 nm, and at 366 nm in the liquid phase (Figure 1).

Interestingly, the red shift and broadening of the absorption peak can also be observed in the absorption profile of the sprayed AuNPs (Figure 2). In particular, the peak absorption of the AuNPs in suspension is located at 529 nm, while the AuNPs coating is characterized by a plateau of local maximum absorption starting around 550 nm (Figure 2). A second peak can also be observed, at a wavelength slightly higher than the plateau, which probably corresponds to aggregates of several nanoparticles that are also visible in SEM images taken from the sample (Figure S1). Indeed, although the spraying of colloidal nanoparticles is a commonly used method for SALDI-MS sample preparation, due to its relative ease of implementation and the wide range of nanosubstrates commercially available, this preparation technique still suffers from limitations, in particular the aggregation and delocalization of the nanoparticles on the support, in this case, a glass slide.[8] The aggregation and delocalization of the nanoparticles could however be limited by modifying the support properties (i.e., the properties of the glass slide surface) by, for example, tuning the surface interaction forces or the chemical affinity between the nanoparticles and the support surface, or by locally heating the nanoparticles, inducing their thermal motion.[35] In the present study, we attempted to limit the gold nanoparticle aggregation and delocalization by optimizing the spraying parameters (e.g., flow rate, nanoparticle solvent, and concentration) but remained limited by the performance of the sprayer used for the sample preparation. The spectrophotometric measurements confirm that the peak absorption of the

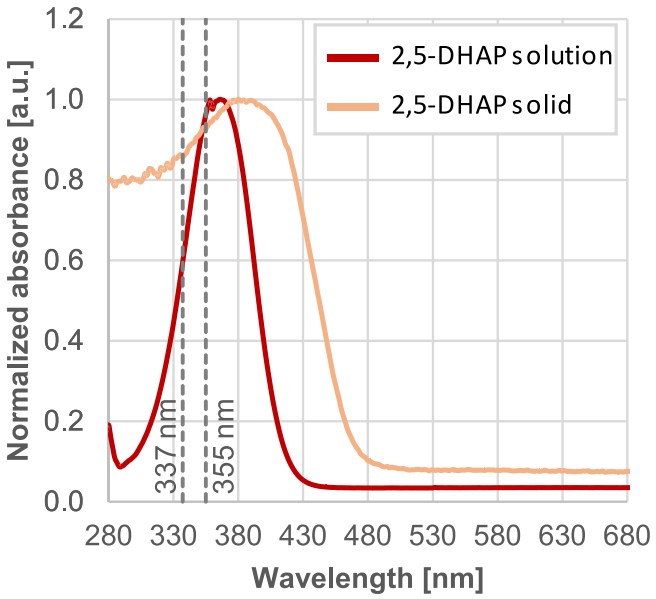

FIGURE 1 Absorption profiles of the 2,5-DHAP matrix in solution (λ_{max} = 366 nm) and in the solid state (λ_{max} = 380 nm). Standard laser wavelengths employed in LDI-MS experiments are displayed. [Color figure can be viewed at wileyonlinelibrary.com]

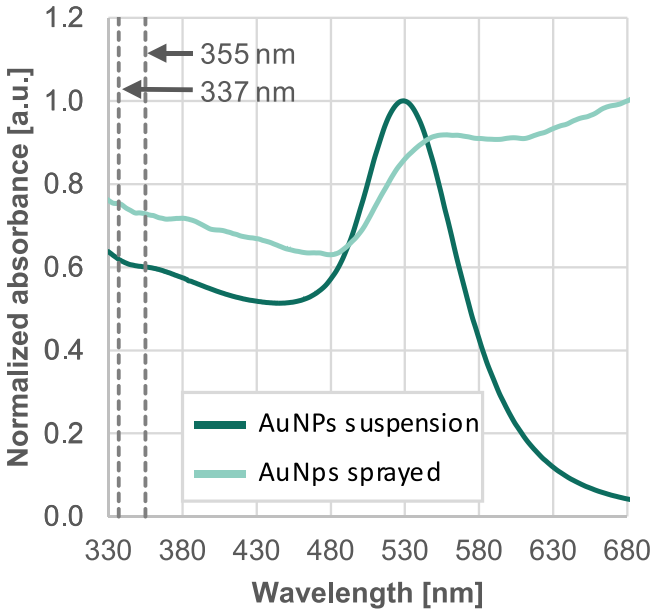

FIGURE 2 Absorption profiles of the gold nanoparticles in suspension (λ_{max} = 529 nm) and when sprayed on a microscope glass slide (λ_{max} = 680 nm, with a plateau > ca. 550 nm). Standard laser wavelengths employed in LDI-MS experiments are displayed. [Color figure can be viewed at wileyonlinelibrary.com]

nanosubstrates strongly differs from the standard MALDI-MS laser wavelengths (i.e., 337 or 355 nm).

3.2 | Assistance of the gold nanoparticles

The effect of the AuNPs on the arginine ion yield was then evaluated at 380 nm. To this end, L-Arginine was analyzed without any assisting material in LDI-MS, and with the gold nanoparticles by SALDI-MS. Figure 3 shows that even if a small number of arginine ions can be produced by LDI-MS, the presence of the gold nanoparticles greatly boosts the ion yield, increasing the protonated arginine ion intensity by about three orders of magnitude.

3.3 | Arginine ion signal intensities as a function of laser wavelength and pulse energy

In this study, we decided to investigate the impact of the laser fluence and wavelength in SALDI-MS, using gold nanoparticles as nanosubstrates, and arginine as a model analyte. Several reasons drove the selection of arginine. Firstly, this low molecular weight compound (<500 Da) was used as a model because SALDI-MS is more widely used for small molecule analysis, due to lower interference in the low *m/z* range compared to MALDI-MS. Secondly, amino acids are the building blocks of various biopolymers, especially peptides and proteins. In future studies, arginine molecules could therefore be used to investigate the impact of the analyte structure on the SALDI fundamental mechanisms. The analysis of peptides composed of an increasing number of arginine monomers could provide valuable insights into the impact of the analyte molecular mass and analyte-surface interaction on the SALDI fundamental mechanisms. Furthermore, amino acids are characterized by a wide range of physicochemical properties, depending on the type of their side chains (i.e., polar, non-polar, acidic, basic, aromatic). Therefore, they are interesting model molecules to probe the impact of the analyte properties on the SALDI processes. Finally, arginine, in particular, is easily ionizable in SALDI-MS using AuNPs, does not extensively fragment, and has no pronounced absorbance in the studied wavelength range. This way any contribution from a possible direct photoionization mechanism resulting from the analyte direct absorbance of the laser could be eliminated.

In Figure 4, the SALDI signal intensity of the protonated arginine ions (*m/z* 175.1) is plotted as a function of the laser wavelength and pulse energy. For each graph, a linear regression was fitted to the data, in the region where the intensity of the protonated arginine ions apparently increases linearly with the laser fluence. The equation of the linear regression allows retrieving what we will define as (i) the laser fluence threshold for ion production and (ii) ionization efficiency. In our model, the laser fluence threshold for ion production can be derived from the intersection of the linear regression with the abscissa, and the slope of the trend line can be interpreted as a first-order representation of the ionization efficiency. Threshold and slope

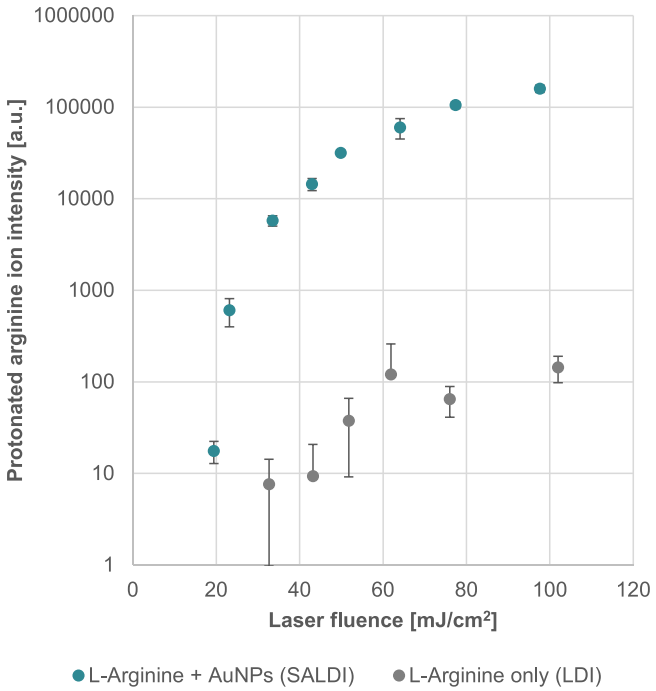

FIGURE 3 Intensity of the protonated arginine ions (m/z 175.1) as a function of the laser fluence, acquired at 380 nm in LDI-MS without any assisting material and in SALDI-MS using gold nanoparticles. [Color figure can be viewed at wileyonlinelibrary.com]

values for each investigated wavelength, as well as associated laser photon energy, are reported in Table 1.

3.3.1 | Laser fluence thresholds for ion production

In SALDI-MS, the lowest threshold value for ion production was obtained at 580 nm (13.40 mJ/cm^2), while the highest value was obtained at 630 nm. However, the threshold value obtained at 630 nm (i.e., 89.15 mJ/cm^2) should be treated with caution as it is particularly high (i.e., almost twice as high as the second highest value, obtained at 480 nm, i.e., 37.67 mJ/cm^2) (Table 1). To assess whether the threshold values are related to the absorption properties of the AuNPs, the mean optical penetration depth, which corresponds to the inverse of the absorbance, and the threshold values obtained at the studied wavelengths were plotted on the same figure. Figure 5 shows a good correlation between the mean penetration depth (of the laser in the AuNPs sprayed on the glass slide) and the threshold values, from 310 to 580 nm (the threshold value at 630 nm is outside the scale). In particular, the maximal and minimal threshold values at 480 and 580 nm, respectively, correspond to the gold nanoparticles absorption minima or maxima.

In contrast to all other investigated wavelengths, the threshold value obtained at 630 nm does not match the absorbance profile but is significantly higher than expected. While a value matching the absorption profile would be expected around 13 mJ/cm^2 the obtained value is 89.15 mJ/cm^2 (see Table 1). It can be speculated that the

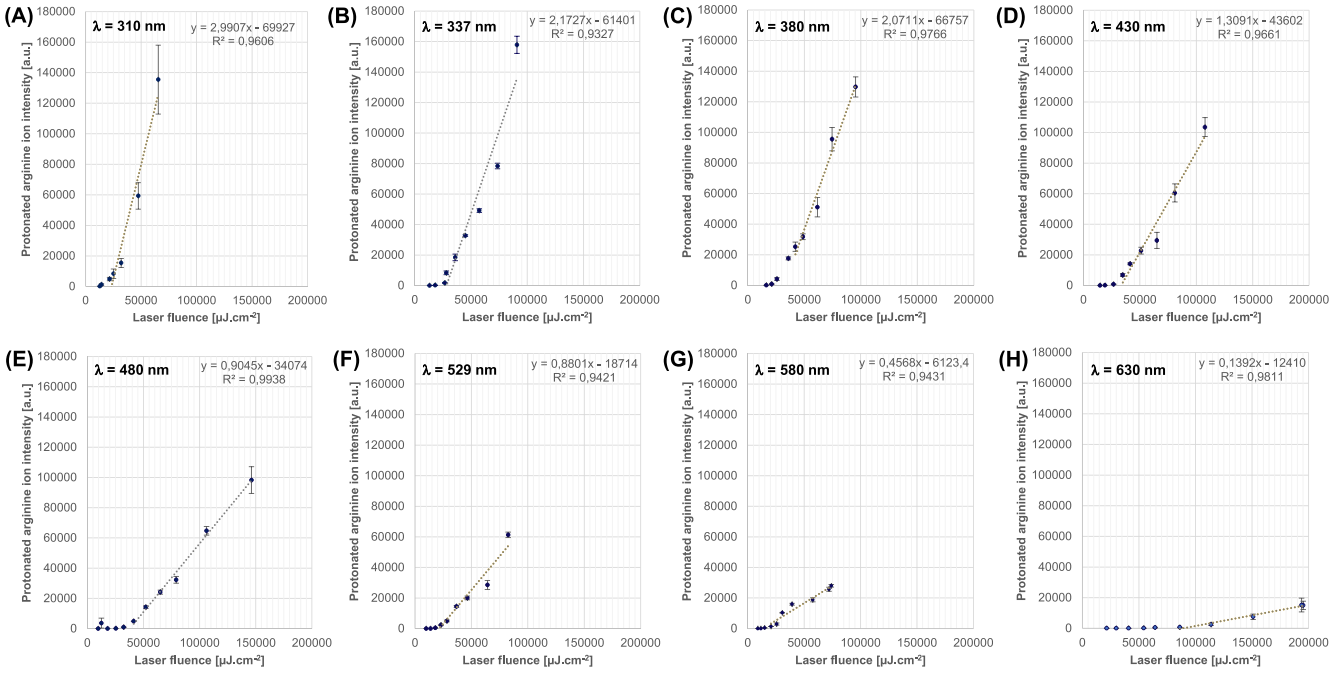

FIGURE 4 Intensity of the protonated arginine ions (m/z 175.1) as a function of the laser fluence, acquired in SALDI-MS using gold nanoparticles, at different laser irradiation wavelengths, namely 310 nm (A), 337 nm (B), 380 nm (C), 430 nm (D), 480 nm (E), 529 nm (F), 580 nm (G), and 630 nm (H). Error bars represent the standard deviation (±1 SD), calculated from three distinct measurements. [Color figure can be viewed at wileyonlinelibrary.com]

Wavelength [nm]	Photon energy [eV]	Threshold [mJ/cm^2]	Slope [a.u.]
310	4.00	23.38	2.9907
337	3.68	28.26	2.1727
380	3.26	32.23	2.0711
430	2.89	33.31	1.3091
480	2.58	37.67	0.9045
529	2.35	21.26	0.8801
580	2.14	13.40	0.4568
630	1.97	89.15	0.1392

TABLE 1 Studied laser wavelengths (and corresponding photon energy) with associated threshold and slope values retrieved from the linear regressions fitted to the data shown in Figure 3.

absorbance measured at this wavelength probably corresponds to gold nanoparticle aggregates (see Figure S1), which might behave differently in SALDI-MS than "isolated" nanoparticles. In particular, the absorption profile of the gold nanoparticles in suspension shows a sharp drop in absorbance starting at 530 nm (Figure 2). Considering the broadening and red shift of the absorption peak, a sharp decrease in the AuNPs absorbance could be envisaged beyond ~ 550 nm (i.e., the maximum of the absorption peak of the "isolated" sprayed gold nanoparticles). Peak deconvolution performed with the evaluation version of LabSpec 5 (*HORIBA Scientific*) indeed suggests several contributions to the absorbance profile, with a peak centered around 548 nm, which shows a drop in absorption after 548 nm, and a minimum around 638 nm (Figure 6).

The apparent correlation between the absorbance of isolated AuNPs on glass and the laser intensity threshold for the appearance of arginine ions strongly suggests that the threshold for desorption is directly linked to the absorption of the laser energy and its rapid dissipation into heat. The SALDI desorption process has indeed been widely recognized as a laser-induced thermal-driven phenomenon.[20,21,36] In this mechanism, the ion desorption results from the rapid heating of the nanosubstrate surface, coupled with heat confinement effects,[21] upon laser irradiation.[20,37] Therefore, nanosubstrates characterized by a strong absorbance in the UV–visible region (when UV irradiation is used), a low heat capacity and a reduced thermal conductivity might induce efficient desorption, and signal enhancement in SALDI-MS.[21,37] In particular, the obtained threshold values correspond to rather low laser fluences. Lai and coworkers previously proposed that when the gold nanoparticles remain solid or liquid (below ~ 45 mJ/cm^2 when 2.5 nm AuNPs are used), the ion desorption is mainly driven by the thermal desorption

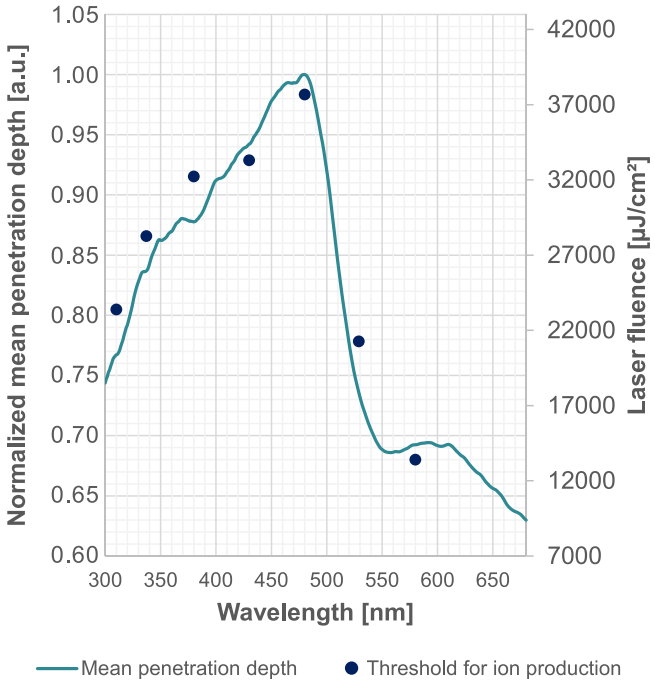

FIGURE 5 Laser mean optical penetration depth (inverse of the AuNPs absorbance) and threshold values for arginine ion production, as a function of the laser wavelength. [Color figure can be viewed at wileyonlinelibrary.com]

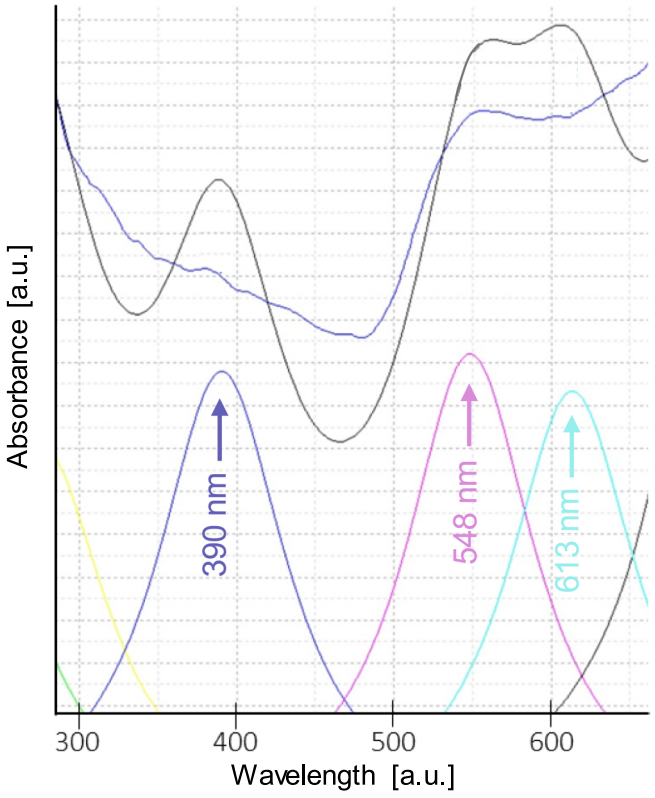

FIGURE 6 Peak deconvolution of the absorption profile of the gold nanoparticles sprayed on a glass slide. [Color figure can be viewed at wileyonlinelibrary.com]

process.[36] This is confirmed by the calculations of Pyatenko and coworkers, which concluded that the photothermal mechanism prevails at low laser intensities.[38]

3.3.2 | Arginine ion yields

Slope values of the linear trend lines (Figure 4) obtained in SALDI-MS that correspond to the ionization efficiency were also plotted as a function of the laser wavelength (green bars in Figure 7), and compared to the data obtained in MALDI-MS using 2,5-DHAP (red bars in Figure 7). In MALDI-MS, the ionization efficiency correlates with the absorption profile of the 2,5-DHAP matrix, with high protonated arginine ion yields around the absorption maximum of the matrix (i.e., 380 nm), and a sharp decrease in the ion yield at higher wavelengths. Almost no arginine ions can be detected above 430 nm. Figures S2 and S3, respectively, show the superposition of the obtained threshold values with mean penetration depth and obtained slope values with the absorption profile of the 2,5-DHAP matrix. In SALDI-MS, the slope values surprisingly do not correlate with the absorbance profile of the AuNPs, and present a linear decrease with increasing laser wavelength (Figure 7). Interestingly, this effect translates to a direct linear correlation of the ionization efficiency with the photon energy at the employed laser wavelengths (Figure 8).

The presented data reveal strong apparent differences between the ionization mechanisms in MALDI and SALDI. The linear dependence of the ionization efficiency on photon energy in SALDI-MS, which is independent of the absorptivity of the AuNPs, points towards a process independent of the thermally driven step of material ejection. It may be speculated that the production of low-energy photoelectrons as recently observed for UV photolysis of DNA attached to AuNPs, may play a role in the ionization mechanism.[39] Further experiments beyond the scope of this initial study are, however, needed to consolidate this hypothesis.

Based on the apparent differences in the ionization mechanisms, SALDI-MS seems more versatile than MALDI-MS with regard to the employed laser wavelength. Although the arginine ion intensity is much lower in SALDI-MS than at optimal laser wavelength in MALDI-MS, ion detection is possible throughout the entire studied wavelength range. Therefore, wavelength adjustments could be performed in SALDI-MS instrumentation, for example, to optimize the analysis of compounds photo-ionizable at wavelengths different from 337 nm and 355 nm or compounds subject to photo-cleavage at 337 or 355 nm.

3.4 | Reproducibility

The reproducibility of the SALDI-MS measurements was assessed. To this end, three experiments were carried out at 380 nm. For each experiment, the laser alignment was re-optimized and a new sample preparation was carried out. The intensity of the protonated arginine

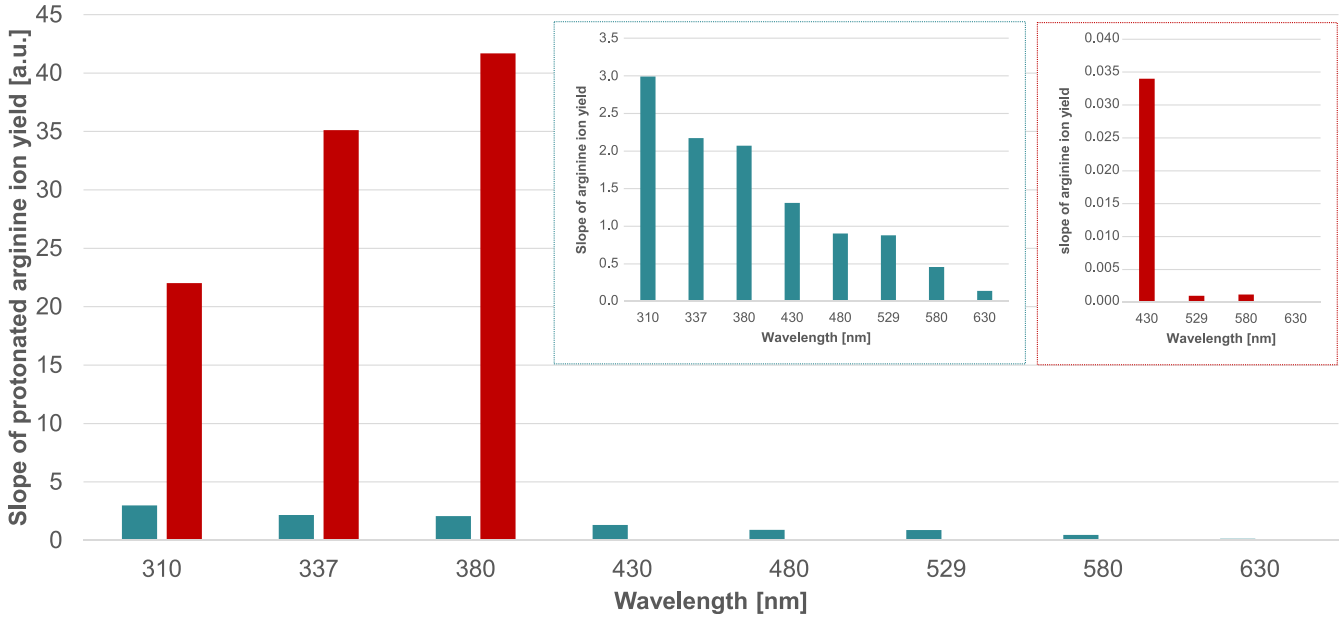

FIGURE 7 Slope values (as an indication of the arginine ionization efficiency) retrieved from SALDI-MS measurement using gold nanoparticles (green) and from MALDI-MS using 2,5-DHAP (red), as a function of the laser wavelength. [Color figure can be viewed at wileyonlinelibrary.com]

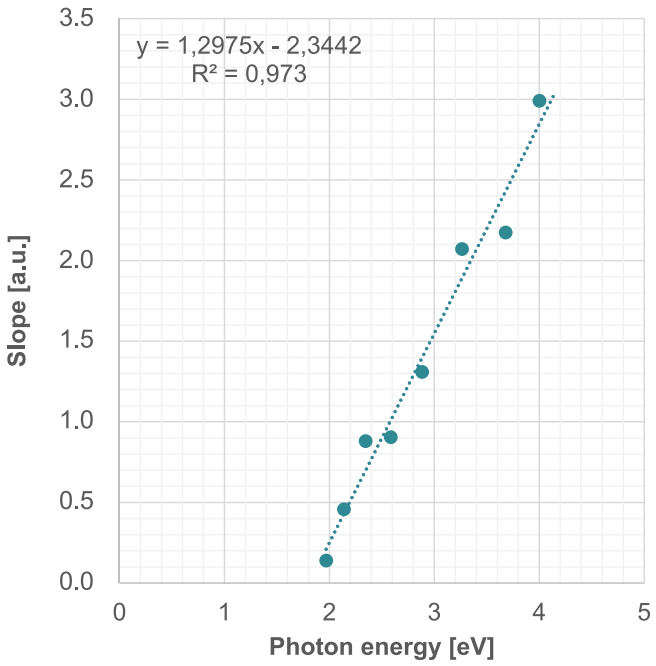

FIGURE 8 Slope values representative of the arginine ionization efficiency retrieved from SALDI-MS measurements using gold nanoparticles, as a function of the laser photon energy at the studied corresponding wavelengths. [Color figure can be viewed at wileyonlinelibrary.com]

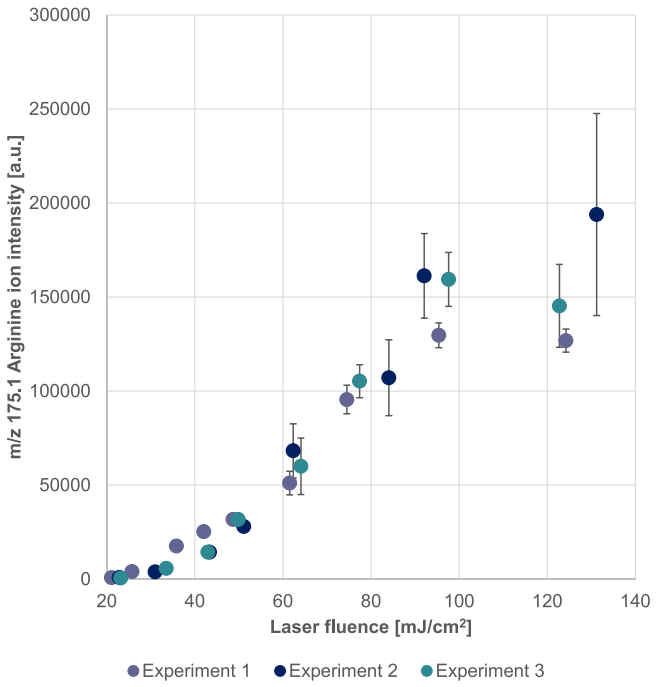

FIGURE 9 Intensity of the protonated arginine ions (m/z 175.1) as a function of the laser fluence, acquired at 380 nm in SALDI-MS using gold nanoparticles in three different experiments. Error bars represent the standard deviation (±1 SD), calculated from three distinct measurements. [Color figure can be viewed at wileyonlinelibrary.com]

ions (*m/z* 175.1) acquired in each experiment is shown in Figure 9. Linear regressions were applied to the data as previously described to extract slope and threshold values (Table 2). The coefficient of variation of the slope values is equal to 15.6% and 10.9% for the threshold values. These data show that the measurements are reproducible, even with slight adjustments of the laser and optics, and sample preparation between the sample runs.

TABLE 2 Threshold and slope values retrieved from the linear regressions fitted to the data shown in Figure 9.

#experiment	Slope [a.u.]	Threshold [mJ.Cm^{-2}]
Experiment 1	2.0711	32.23
Experiment 2	2.8119	39.63
Experiment 3	2.6723	38.63

4 | CONCLUSION

The performed wavelength study, covering eight data points between 310 and 630 nm, hence covering the classical UV MALDI-MS as well as almost the full visible regime, offers new interesting insights into the mechanisms of SALDI-MS with gold nanoparticles. For the analyte test system (i.e., arginine molecules, spray-coated onto the AuNPs coating) our data fully corroborate a thermal desorption model for material ejection and present new insights into the mechanism of ionization. The study revealed strong variations between the laser wavelength dependence in SALDI and MALDI MS regarding the correlation of both material ejection and ionization efficiency with the absorptivity of the assisting material (either the AuNPs in SALDI-MS or the 2,5-DHAP matrix in MALDI-MS).

Altogether, our fundamental investigations suggest possible avenues for improving SALDI-MS upon wavelength adjustment, for example in the analysis of UV-sensitive compounds or to specifically trigger photochemical reactions. A readily available wavelength for such studies, which would also match the peak absorption of the AuNPs would be that of the frequency-tripled Nd:YAG laser (532 nm). Future studies to further evaluate this potential should include alternative analyte systems (next to the studied arginine amino acid of particular high proton affinity). Indeed, the transferability of the obtained results to other analyte systems has to be demonstrated. Further studies should focus on the study of the impact of the analyte molecular weight on the SALDI fundamental mechanisms, for example, by analyzing peptides composed of a different number of arginine monomers, as suggested above. In addition, future studies may also include analyte systems characterized by a variety of physicochemical properties, as well as other nanosubstrates (e.g., with different morphologies and/or chemical nature).

AUTHOR CONTRIBUTIONS

Wendy H. Müller: Conceptualization; writing—original draft; validation; visualization; writing—review and editing; investigation; data curation; methodology; formal analysis; funding acquisition. **Alexander Potthoff:** Methodology; writing—review and editing; software; investigation; validation. **Klaus Dreisewerd:** Conceptualization; funding acquisition; writing—review and editing; resources. **Jens Soltwisch:** Conceptualization; investigation; writing—original draft; methodology; writing—review and editing; resources; validation.

ACKNOWLEDGMENTS

WHM acknowledges a postdoctoral research fellowship by the Alexander von Humboldt Foundation. We thank Benjamin Thomas (Shimadzu Europa GmbH, Duisburg) for technical support in UV–Vis spectroscopy measurements and Harald Nüsse (Institute of Medical Physics and Biophysics) for SEM images. Open Access funding enabled and organized by Projekt DEAL.

DATA AVAILABILITY STATEMENT

The data that support the findings of this study are available from the corresponding author upon reasonable request.

CONFLICT OF INTEREST

The authors declare no conflict of interest.

ORCID

Jens Soltwisch https://orcid.org/0000-0002-0258-1561

REFERENCES

1. Karas M, Bachmann D, Hillenkamp F. Matrix-assisted ultraviolet laser desorption of non-volatile compounds. *Int J Mass Spectrom Ion Process*. 1987;78:53-68. doi:10.1016/0168-1176(87)87041-6
2. Dreisewerd K. Recent methodological advances in MALDI mass spectrometry. *Anal Bioanal Chem*. 2014;406(9-10):2261-2278. doi:10.1007/s00216-014-7646-6
3. Karas M, Bachmann D, Hillenkamp F. Influence of the wavelength in high-irradiance ultraviolet laser desorption mass spectrometry of organic molecules. *Anal Chem*. 1985;57:2935-2939.
4. Dreisewerd K. The desorption process in MALDI. *Chem Rev*. 2003;103(2):395-425. doi:10.1021/cr010375i
5. Calvano CD, Monopoli A, Cataldi TRI, Palmisano F. MALDI matrices for low molecular weight compounds: an endless story? *Anal Bioanal Chem*. 2018;410(17):4015-4038. doi:10.1007/s00216-018-1014-x
6. Law KP, Larkin JR. Recent advances in SALDI-MS techniques and their chemical and bioanalytical applications. *Anal Bioanal Chem*. 2011;399(8):2597-2622. doi:10.1007/s00216-010-4063-3
7. Müller WH, De Pauw E, Far J, Malherbe C, Eppe G. Imaging lipids in biological samples with surface-assisted laser desorption/ionization mass spectrometry: a concise review of the last decade. *Prog Lipid Res*. 2021;83:101114. doi:10.1016/j.plipres.2021.101114
8. Müller WH, Verdin A, De Pauw E, Malherbe C, Eppe G. Surface-assisted laser desorption/ionization mass spectrometry imaging: a review. *Mass Spectrom Rev*. 2022;41(3):373-420. doi:10.1002/mas.21670
9. Müller WH, McCann A, Arguelles Arias A, et al. Imaging metabolites in agar-based bacterial co-cultures with minimal sample preparation using a DIUTHAME membrane in surface-assisted laser desorption/ionization mass spectrometry. *Chemistry Select*. 2022;7(18):e202200734. doi:10.1002/slct.202200734
10. Müller WH, Verdin A, Kune C, et al. Dual polarity SALDI FT-ICR MS imaging and Kendrick mass defect data filtering for lipid analysis. *Anal Bioanal Chem*. 2021;413(10):2821-2830. doi:10.1007/s00216-020-03020-w
11. Schürenberg M, Dreisewerd K, Kamanabrou S, Hillenkamp F. Influence of the sample temperature on the desorption of matrix molecules and ions in matrix-assisted laser desorption ionization. *Int. J. Mass Spectrom. Ion Process*. 1998;172(1-2):89-94. doi:10.1016/S0168-1176(97)00253-X

12. Müller WH. Optimization of surface-assisted laser desorption/ionization mass spectrometry. *Bull la Société R Ddes Sci Liège*. 2022;91(1):105-127. doi:10.25518/0037-9565.10993
13. Bae YJ, Kim MS. A thermal mechanism of ion formation in MALDI. *Annu Rev Anal Chem*. 2015;8(1):41-60. doi:10.1146/annurev-anchem-081413-024102
14. Karas M, Krüger R. Ion formation in MALDI: the cluster ionization mechanism. *Chem Rev*. 2003;103(2):427-439. doi:10.1021/cr010376a
15. Knochenmuss R. Ion formation mechanisms in UV-MALDI. *Analyst*. 2006;131:966-986. doi:10.1039/b605646f
16. Lee C, Inutan ED, Chen JL, et al. Toward understanding the ionization mechanism of matrix-assisted ionization using mass spectrometry experiment and theory. *Rapid Commun Mass Spectrom*. 2021;35(S1):e8382. doi:10.1002/rcm.8382
17. Zenobi R, Knochenmuss R. Ion formation in MALDI mass spectrometry. *Mass Spectrom Rev*. 1998;17(5):337-366. doi:10.1002/(SICI)1098-2787(1998)17:53.0.CO,2-S
18. Jaskolla TW, Karas M. Compelling evidence for lucky survivor and gas phase protonation: the unified MALDI Analyte protonation mechanism. *J am Soc Mass Spectrom*. 2011;22(6):976-988. doi:10.1007/s13361-011-0093-0
19. Xiao Y, Retterer ST, Thomas DK, Tao J-Y, He L. Impacts of surface morphology on ion desorption and ionization in desorption ionization on porous silicon (DIOS) mass spectrometry. *J Phys Chem C*. 2009;113(8):3076-3083. doi:10.1021/jp808844f
20. Ng K, Chau S, Tang H, et al. Ion-desorption efficiency and internal-energy transfer in surface-assisted laser desorption/ionization: more implication(s) for the thermal-driven and phase-transition-driven desorption process. *J Phys Chem C*. 2015;119(41):23708-23720. doi:10.1021/acs.jpcc.5b05957
21. Picca RA, Calvano CD, Cioffi N, Palmisano F. Mechanisms of nanophase-induced desorption in LDI-MS. *A Short Review. Nanomaterials*. 2017;7(4):75. doi:10.3390/nano7040075
22. Soltwisch J, Jaskolla TW, Dreisewerd K. Color matters - material ejection and ion yields in UV-MALDI mass spectrometry as a function of laser wavelength and laser fluence. *J am Soc Mass Spectrom*. 2013;24(10):1477-1488. doi:10.1007/s13361-013-0699-5
23. Niehaus M, Schnapp A, Koch A, Soltwisch J, Dreisewerd K. New insights into the wavelength dependence of MALDI mass spectrometry. *Anal Chem*. 2017;89(14):7734-7741. doi:10.1021/acs.analchem.7b01744
24. Soltwisch J, Jaskolla TW, Hillenkamp F, Karas M, Dreisewerd K. Ion yields in UV-MALDI mass spectrometry as a function of excitation laser wavelength and optical and physico-chemical properties of classical and halogen-substituted MALDI matrixes. *Analytical*. 2012;84:6567-6576. doi:10.1021/ac3008434
25. Knochenmuss R, Zenobi R. MALDI ionization: the role of in-plume processes. *Chem Rev*. 2003;103(2):441-452. doi:10.1021/cr0103773
26. Wiegelmann M, Dreisewerd K, Soltwisch J. Influence of the laser spot size, focal beam profile, and tissue type on the lipid signals obtained by MALDI-MS imaging in oversampling mode. *J am Soc Mass Spectrom*. 2016;27(12):1952-1964. doi:10.1007/s13361-016-1477-y
27. Robinson KN, Steven RT, Race AM, Bunch J. The influence of MS imaging parameters on UV-MALDI desorption and ion yield. *J am Soc Mass Spectrom*. 2019;30(7):1284-1293. doi:10.1007/s13361-019-02193-8
28. Guenther S, Koestler M, Schulz O, Spengler B. Laser spot size and laser power dependence of ion formation in high resolution MALDI imaging. *Int. J. Mass Spectrom.* 2010;294(1):7-15. doi:10.1016/j.ijms.2010.03.014
29. Wiegelmann M, Soltwisch J, Jaskolla TW, Dreisewerd K. Matching the laser wavelength to the absorption properties of matrices increases the ion yield in UV-MALDI mass spectrometry. *Anal Bioanal Chem*. 2013;405(22):6925-6932. doi:10.1007/s00216-012-6478-5
30. Potthoff A, Dreisewerd K, Soltwisch J. Detailed characterization of the postionization efficiencies in MALDI-2 as a function of relevant input parameters. *J Am Soc Mass Spectrom*. 2020;31(9):1844-1853. doi:10.1021/jasms.0c00072
31. Chambers MC, Maclean B, Burke R, et al. A cross-platform toolkit for mass spectrometry and proteomics. *Nat Biotechnol*. 2012;30(10):918-920. doi:10.1038/nbt.2377
32. Schramm T, Hester Z, Klinkert I, Both J, et al. ImzML — a common data format for the flexible exchange and processing of mass spectrometry imaging data. *J Proteomics*. 2012;75(16):5106-5110. doi:10.1016/j.jprot.2012.07.026
33. Race AM, Styles IB, Bunch J. Inclusive sharing of mass spectrometry imaging data requires a converter for all. *J Proteomics*. 2012;75(16):5111-5112. doi:10.1016/j.jprot.2012.05.035
34. Fay, D. pyimzML parser for the imzML format https://github.com/alexandrovteam/pyimzML (accessed Jun 22, 2024), doi:10.1016/j.shpsa.2024.06.004.
35. Escorcia-Diaz D, Garcia-Mora S, Rendon-Castrillon L, Ramirez-Carmona M, Ocampo-Lopez C. Advancements in nanoparticle deposition techniques for diverse substrates: a review. *Nanomaterials*. 2023;13(18):2586. doi:10.3390/nano13182586
36. Lai SKM, Tang H, Lau K, Ng K. Nanosecond UV laser ablation of gold nanoparticles: enhancement of ion desorption by thermal-driven desorption, vaporization, or phase explosion. *J Phys Chem C*. 2016;120(36):20368-20377. doi:10.1021/acs.jpcc.6b06261
37. Song K, Cheng Q. Desorption and ionization mechanisms and signal enhancement in surface assisted laser desorption ionization mass spectrometry (SALDI-MS). *Appl Spectrosc Rev*. 2020;55(3):220-242. doi:10.1080/05704928.2019.1570519
38. Pyatenko A, Yamaguchi M, Suzuki M. Mechanisms of size reduction of colloidal silver and gold nanoparticles irradiated by Nd:YAG laser. *J Phys Chem C*. 2009;113(21):9078-9085. doi:10.1021/jp808300q
39. Huwaidi A, Robert G, Kumari B, et al. Electron-induced damage by UV photolysis of DNA attached to gold nanoparticles. *Chem Res Toxicol*. 2024;37(2):419-428. doi:10.1021/acs.chemrestox.3c00370

SUPPORTING INFORMATION

Additional supporting information can be found online in the Supporting Information section at the end of this article.

How to cite this article: Müller WH, Potthoff A, Dreisewerd K, Soltwisch J. Investigation of the laser fluence and wavelength dependence in surface-assisted laser desorption/ionization mass spectrometry using gold nanoparticles. *Rapid Commun Mass Spectrom*. 2024;e9895. doi:10.1002/rcm.9895